Available online at www.sciencedirect.com
SCIENCE DIRECT®
Acta Materialia 52 (2004) 773–784
Acta MATERIALIA
www.actamat-journals.com

Discrete dislocation simulation of plastic deformation in metal thin films

Burghard von Blanckenhagen [a,b], Eduard Arzt [a], Peter Gumbsch [b,c,*]

[a] *Max-Planck-Institut für Metallforschung, Heisenbergstr. 3, D-70569 Stuttgart, Germany*
[b] *Universität Karlsruhe, Institut für Zuverlässigkeit von Bauteilen und Systemen, Kaiserstr. 12, D-76131 Karlsruhe, Germany*
[c] *Fraunhofer Institut für Werkstoffmechanik, Freiburg und Halle, Wöhlerstr. 11, D-79108 Freiburg, Germany*

Received 12 March 2003; received in revised form 1 October 2003; accepted 7 October 2003

Abstract

The plastic deformation of polycrystalline fcc metal thin films with thicknesses of 1 μm and less is investigated by simulating the dynamics of discrete dislocations in a representative columnar grain. The simulations are based on the assumption that dislocation sources or multiplication sites are rare and that every source has to operate several times to generate appreciable plastic deformation. This model is thoroughly tested by calculating the response of randomly distributed dislocation sources to an applied stress and comparing the results with experimental data. Stress–strain curves, dislocation densities, work hardening rates and their dependence on the film thickness are calculated. The agreement between simulation and experiment is good and many aspects of thin film plasticity can be understood with the assumption that small-scale plastic deformation is source controlled rather than mobility controlled.
© 2003 Acta Materialia Inc. Published by Elsevier Ltd. All rights reserved.

PACS: 68.60.Bs; 61.72.Lk; 46.15.−x

Keywords: Thin films; Plastic deformation; Dislocation; Simulation

1. Introduction

The progressive miniaturization in micro-electronics and micro-mechanics has led to a drastic reduction of the dimensions of the components in these devices. Interconnects in integrated circuits or tiny "structural parts" in micro-electro-mechanical (MEMS) devices made from metallic materials often have thicknesses of the order 1 μm or below. Due to the confinement in (at least) one dimension, the mechanical properties of these films differ dramatically from their bulk counterparts. Understanding the mechanical properties of thin metal films is therefore crucial in predicting the reliability of such small-scale devices.

Experiments have shown that the flow stresses of thin metal films can exceed those of the corresponding bulk material by an order of magnitude and increase with decreasing film thickness [1–5]. To comprehend the plastic deformation of thin films at room temperature, it is necessary to study the effect of the confined geometry on the dislocation multiplication and motion. Grain size and film thickness of the films treated here are much smaller than the characteristic length scales of dislocation networks observed in bulk material after deformation. Indeed, dislocation cell structures have not been observed in thin films [6]. The collective behavior of many interacting dislocations, which would lead to the formation of cell structures, is impeded by grain boundaries and interfaces. Therefore, the number of dislocations which have to be considered in order to understand thin film plasticity is rather small and computer simulation of the deformation becomes possible. A three-dimensional discrete dislocation dynamics simulation (DDD) is used here to study thin film deformation by investigating dislocation motion in a representative columnar grain. Randomly distributed

* Corresponding author. Tel.: +49-761-514-2100; fax: +49-761-514-2400.
E-mail address: gumbsch@iwm.fraunhofer.de (P. Gumbsch).

1359-6454/$30.00 © 2003 Acta Materialia Inc. Published by Elsevier Ltd. All rights reserved.
doi:10.1016/j.actamat.2003.10.022

Frank–Read sources in the grain interior are used as the initial dislocation configuration. While the operation of a single Frank–Read source in the confined geometry of a thin film was investigated in previous papers [7,8], this work also includes the interaction between dislocations from different sources, the activation of different sources at different stresses and the effect of the random distribution of the sources in the grain.

Stress–strain curves are calculated with the simulation and several experimentally determined quantities, which show characteristic thin film behavior, are compared with the simulated results. The aspects which are juxtaposed are: the stress at a given plastic strain which increases with decreasing film thickness [1–5]; hardening rates which are exceptionally high for thin films and increase with decreasing film thickness [9,10]; the onset of plastic deformation during unloading, which shows a pronounced Bauschinger effect for thin films [11–13]. Furthermore, results from in situ transmission electron microscopy (TEM) studies of thin film deformation are compared with the simulation.

The paper is organized as follows: first, the DDD simulation method is outlined (Section 2 and Appendix A). The results of the simulations are presented in Section 3 and discussed and compared with experimental data in Section 4.

2. Method

The simulation is based on linear isotropic elasticity where dislocations are considered as line defects in a continuum. The discrete dislocations are represented by nodes connected by straight segments of mixed character. The force on each node is calculated from the local stress using the Peach–Koehler equation. The local stress consists of the applied stress and stresses generated by the presence of the dislocations themselves. The Peierls stress is neglected because its contribution is negligible for the cases considered [14].

To compute the self-stress of a dislocation, the segments connecting the node of stress calculation with its neighboring nodes are replaced by a circular arc. The stress of the circular arc is calculated using Brown's averaging procedure [15] with an approximation introduced by Schwarz [16]. The stress caused by the remote part of the dislocation and by other dislocations is computed using an analytical expression to determine the stress from the straight segment which connects two nodes [17]. Once the forces on each node are known, the nodes are moved according to a viscous drag law [14]. The dislocations are dynamically rediscretized: nodes are inserted where the curvature of the dislocations is high and deleted where the dislocations are almost straight. Further details of the simulation and test calculations concerning the dislocation self-stress can be found in [18]. The treatment of short-range interactions is described in detail in the Appendix A. The simulation is restricted to low temperatures (room temperature for Al or Cu) where the dislocations move by conservative slip.

Cross-slip was tested in a simplified form, where the dislocations were allowed to cross-slip, if the resolved shear stress on the cross-slip system is larger than on the primary glide system and if the stress is large enough to bow out the part of the dislocation which is of screw character. Cross-slipping of dislocations was observed for cases were two dislocations come close to each other in the interior of the simulated grain. However, the encounters, which lead to cross-slip are very rare. For the strains reached in this study, it was found that the simulated stress–strain curves did not change significantly when including cross-slip. This can be understood since Frank–Read sources are included from the beginning of the simulation (see below) and plastic deformation can be achieved without cross-slip. Therefore, cross-slip is not included in the simulations presented here.

To model the plastic deformation of a polycrystalline thin film, dislocation production and motion in one single columnar grain is simulated. The grain is assumed to have cubic shape with vertical dimension h (film thickness) and horizontal dimension d (grain size). The grain boundaries are introduced as impenetrable obstacles for the dislocations. The interfaces to the bottom and top side of the grain can either be treated as free surfaces to mimic a free-standing film or as impenetrable interfaces. The latter case mimics a metal film sandwiched between a ceramic substrate and a cap layer, where dislocations are deposited at the interfaces. Differences between the elastic moduli of film, cap layer and substrate, which would lead to image forces, are neglected. This approximation is justified because most of the dislocations are located in the grain interior and the self-stress due to the curvature of the dislocations is usually much larger than the image forces [19,20].

In a free-standing film the dislocations can leave the film at the surfaces. A dislocation which touches the surface in the simulation is simply terminated there. The position of the terminating nodes is determined by requiring that the last segment of the dislocation enters the free surface at right angle. This is correct for pure edge and screw dislocations. For mixed dislocations there is a tendency to align the dislocation in the direction of the Burgers vector to minimize line energy [16,21]. However, as long as the critical process is the activation of sources in the grain interior, the treatment of the dislocations close to the surfaces plays only a minor role in determining the flow stress [22]. The importance of image forces in the grain interior was estimated by comparison of stress–strain curves of a free-standing film with and without the correct boundary

conditions at the free surfaces. To establish the correct boundary conditions of the free surfaces, point forces were applied on the surface to compensate for the tractions induced by the dislocations [23]. An interaction between the two free surfaces has also been taken into account following [24]. The calculations with and without the image forces agreed within a few percent. However, the computational time of the simulation with the correct free surface boundary conditions was two orders of magnitude higher [25]. The image forces are therefore neglected in the following simulations of free-standing films.

In order to introduce the dislocations, Frank–Read sources are placed in the grain interior. The sources are realized as dislocation segments which are pinned at both ends. The side-arms, which would lie on secondary slip planes are neglected here because the change in the activation stress of a Frank–Read source due to the stress field of the side-arms has been shown to be small [26]. Test simulations have also shown that the increase in flow stress due to the side-arms acting as additional obstacles for moving dislocations is smaller than the error due to different starting configurations [25].

If not stated otherwise, the size of a source, the position, the orientation and the slip system are chosen randomly. The slip system is selected from the primary slip systems of an fcc crystal, $\langle 1\,1\,0\rangle\{1\,1\,1\}$. A grain with a $(\bar{1}\,\bar{1}\,1)$ slip plane parallel to the surface is simulated because most of the investigated thin films have a pronounced $\langle 1\,1\,1\rangle$ fiber texture [10,27,28]. The rotation around the $[\bar{1}\,\bar{1}\,1]$-axis is chosen randomly.

A homogeneous uniaxial tensile stress is applied parallel to the interfaces and diagonal to the simulation box. The stress is adjusted to maintain a constant mean node velocity (which is equivalent to a constant strain rate). This velocity is set to 30 m s^{-1} as a compromise between quasi-static calculations and the desire to limit computer time [18].

Dislocations move under the applied stress and the resulting plastic strain is recorded. The macroscopic plastic strain tensor $\tilde{\varepsilon}_{\mathrm{pl}}$ is calculated using [29, p. 294]

$$\tilde{\varepsilon}_{\mathrm{pl}} = \sum_{i=1}^{N} \frac{l_i \Delta x_i}{2V} (\mathbf{n}_i \otimes \mathbf{b}_i + \mathbf{b}_i \otimes \mathbf{n}_i), \quad (1)$$

where l_i is the length of the dislocation segment i, Δx_i is the displacement of the segment during a time step, $\mathbf{n}_i$ is the normal vector of the slip plane, $\mathbf{b}_i$ the Burgers vector and V the volume of the simulated crystal. $\otimes$ denotes the dyadic product. N is the total number of dislocation segments. Stress–strain curves are generated by plotting the applied stress vs. the component of the strain tensor which corresponds to a change in length in the direction of the tensile axis. The surmounting of critical dislocation configurations manifests itself in local maxima in the stress–strain curves.

3. Results

In Section 3.1 stress–strain curves are calculated for a system of non-interacting dislocation sources. They are based on two-dimensional simulations of a single source in a grain [8]. Results from three-dimensional simulations with many interacting dislocations are shown in Section 3.2.

3.1. Calculation of stress–strain curves for non-interacting dislocation sources

Fig. 1 displays the stress to activate a single source located at the center of a grain with impenetrable boundaries vs. the size of the source from the first to the sixth activation event. The source activation stress is defined as the stress to produce a loop and to transfer the pinned dislocation segment back to its initial configuration. More details of the calculations displayed in Fig. 1 can be found in [8].

To calculate a stress–strain curve from the data in Fig. 1, it is assumed that sources of different sizes exist in the grain with equal probability. The plastic strain at a given stress level is determined by counting the number of emitted dislocation loops for each source of a given size. Each loop which traverses the grain generates a plastic strain of b/h, and the total plastic strain is given by summing over all emitted loops. Additionally, it is taken into account that sources with $s > h/3$ on average sweep out half of the grain if the applied stress is large enough to activate the Frank–Read source but too small to produce an entire loop. Fig. 2 shows the stress–strain curve calculated from Fig. 1 for a continuous distribution of dislocation sources over all sizes. The plastic strain $\varepsilon_{\mathrm{pl}}$ is normalized by the total number of sources N_0. The first plastic deformation is achieved when

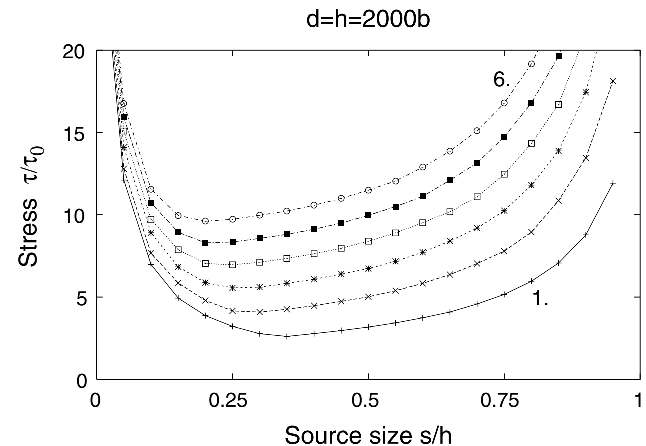

Fig. 1. Source activation stress from the first to the sixth activation event for a dislocation source positioned in the center of a grain with impenetrable boundaries. τ_0 is the stress to activate a source of size $s = h$.

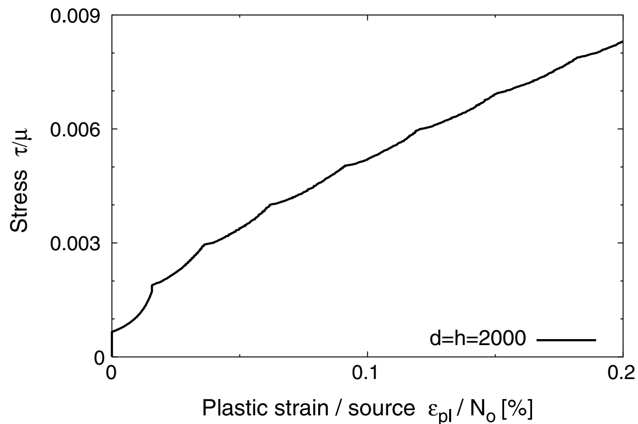

Fig. 2. Stress–strain curve calculated from Fig. 1 for a homogeneous distribution of dislocation source sizes.

sources which completely extend over the film thickness are activated and produce a half loop. The first kink in the curve corresponds to the creation of the first closed dislocation loop, which is characterized by the minimum source activation stress at $s = h/3$ (Fig. 1). The subsequent kinks mark the approach of a new activation branch with an additional source activation.

3.2. Simulations with many sources

Fig. 3 shows different stages in the simulated deformation process of a grain with impenetrable interfaces as an example of a simulation with many dislocation sources. The initial random configuration of pinned source segments is displayed in Fig. 3(a). After loading, the pinned segments expand according to the resolved shear stresses. Dislocations on slip planes which are parallel to the interfaces move only due to the interaction with other dislocations. Dislocation locks are formed and dislocation cutting events are observed. However, at advanced deformation with multiple source activation these short-range interactions do not impede the dislocation motion appreciably. Dislocation loops pile-up at the boundaries (Fig. 3(b)). These impose a back stress on the sources and with increasing applied

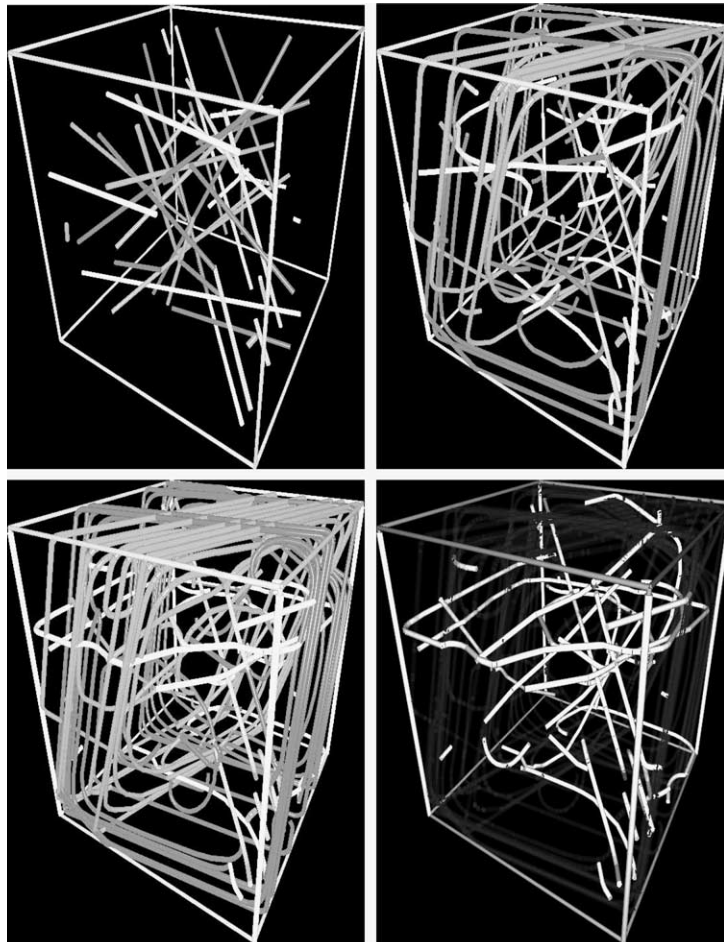

Fig. 3. Initial dislocation configuration (a) and configurations after 0.25% (b), and 0.47% (c) plastic strain. The corresponding dislocation densities are $\rho = 0.44 \times 10^{14}$ m^{-2} (a), $\rho = 2.2 \times 10^{14}$ m^{-2} (b), and $\rho = 4.2 \times 10^{14}$ m^{-2} (c). (d) The inactive dislocation sources that did not produce loops after a plastic strain of 0.47%.

stress other dislocation sources with smaller resolved shear stresses or smaller sizes are activated. Nevertheless, sources of slip systems with Schmid factors close to zero do not produce dislocation loops as can be seen in Fig. 3(d). At 0.47% plastic strain only roughly a quarter of all randomly placed sources have emitted dislocation loops (Fig. 3(c)).

Fig. 4 displays stress vs. plastic strain for a grain with impenetrable interfaces ($d = h = 2000b$) for different numbers of dislocation sources. To facilitate the comparison, only local maxima of the stress–strain curves are plotted. The curves show an initial region where the slope decreases, as more and more dislocation sources are activated. For larger plastic strains, the number of active sources stays almost constant and nearly linear hardening is observed.

The data of Fig. 4 (plus data from additional simulations) are reorganized in Fig. 5 to visualize the dependence on the number of dislocation sources. The simulated stresses at 0.1%, 0.3% and 0.5% plastic strain are shown as a function of the number of dislocation sources N_0. For small N_0 a high stress is needed to achieve a certain plastic strain. The stress decreases for increasing N_0 and stays almost constant for $N_0 > 40$.

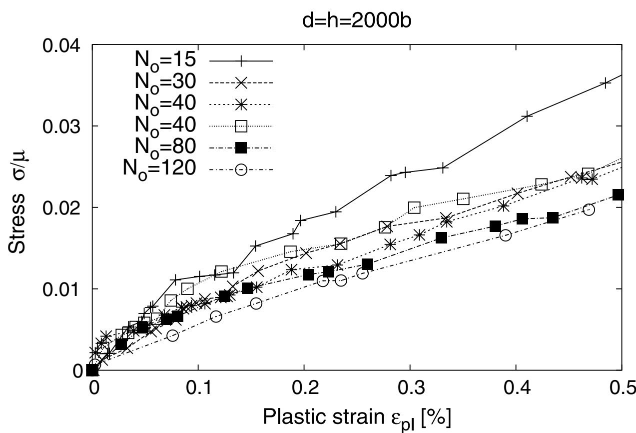

Fig. 4. Stress vs. plastic strain for a grain with the dimensions $d = h = 2000b$. Simulations are shown for different numbers of dislocation sources and different initial configurations of the sources.

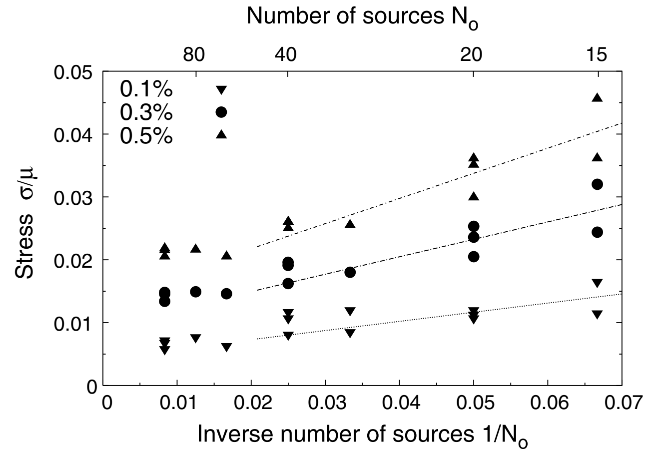

Fig. 5. Stress at 0.1%, 0.3% and 0.5% plastic strain vs. inverse number of dislocation sources in a grain with $d = h = 2000b$. Data points from individual simulations with different random starting configurations are shown. The lines illustrate the $1/N_0$ dependence of the stress for small N_0.

Different starting configurations can lead to different stresses even if the number of dislocation sources is the same. This scatter is due to the limited number of dislocation sources and their random distribution in the grain. The more dislocation sources are in a grain, the more sources will be favorably positioned for activation at a given stress level. A small number of active dislocation sources results in a pronounced work hardening because each source has to operate many times and the dislocation loops deposited at the boundaries exert a back stress on the source.

To minimize the statistical error several runs with different random starting configurations but the same number of dislocation sources are averaged in the following. The statistical error of an averaged stress–strain curve is calculated from the deviations of the distinct runs. Table 1 summarizes these errors at different plastic strains for calculations shown in Figs. 6 and 7. Except

Table 1
Statistical data for stress–strain curves in Figs. 6 and 7

$d = h$	N_0	Number of simulations	Average stress (10^{-3} μm) ± relative error		
			At $\varepsilon_{pl} = 10^{-3}$	At $\varepsilon_{pl} = 3 \times 10^{-3}$	At $\varepsilon_{pl} = 5 \times 10^{-3}$
500b	2–3	16	42 ± 15%	82 ± 19%	114 ± 19%
1000b	10	11	15 ± 9%	25 ± 7%	35 ± 9%
1517b	23	6	8.8 ± 5%	15 ± 4%	21 ± 6%
2000b	40	5	7.8 ± 7%	12 ± 4%	17 ± 5%
3906b	160	2	5.2 ± 4%	7.9 ± 7%	
2000b	40	4	10 ± 8%	17 ± 7%	25 ± 3%

The first row contains the dimensions of the simulated grain, the second the number of dislocation sources and the third the number of runs with different initial random configurations. The stress levels in units of 10^{-3} μm at three different levels of plastic strain are shown together with the relative errors. The latter result from an error estimation for repeated measurements of a statistical quantity following a normal distribution. The first five lines show data for a free-standing film, the last line is for a capped film.

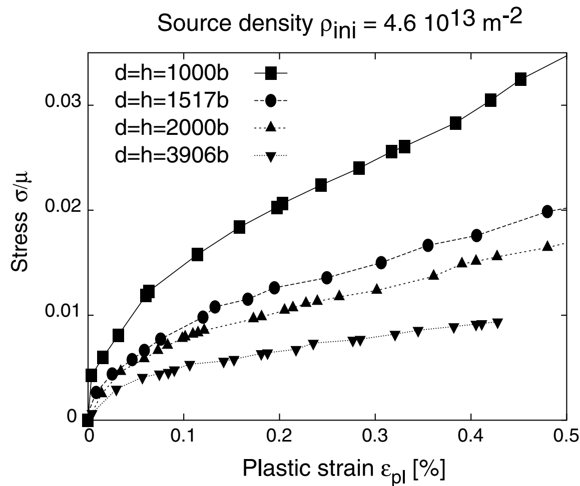

Fig. 6. Stress vs. plastic strain for different film thicknesses at constant source density (free-standing film). The dislocation density corresponds to 10 sources for a grain with $d = h = 1000b$, 40 sources for $d = h = 2000b$ and 160 sources for $d = h = 4000b$. The curves are averages of several simulations with different random start configurations (Table 1).

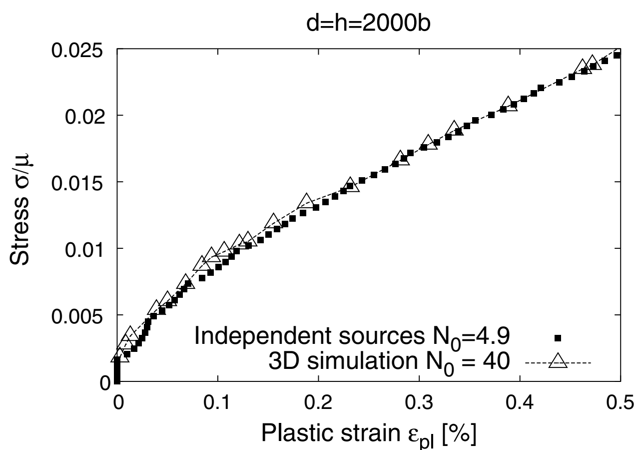

Fig. 7. Stress–strain curve deduced from an independent source calculation (Fig. 2) and fitted via N_0 to a curve, which was calculated in a three-dimensional simulation with many interacting dislocations (capped film, Table 1).

for the thinnest film (which is only used to show the simulated hardening rate at very small h, Fig. 9) the relative errors are smaller than 10%. This is sufficiently small since it is of the same order of magnitude as the error due to the approximative treatment of the dislocation core [16].

Fig. 6 shows stress–strain curves for different film thicknesses and grain sizes ($h = d$). A grain with free surfaces is simulated. The initial dislocation density (i.e., the total length of the straight, pinned dislocation segments divided by the volume of the grain) is held constant at $\rho_{\text{ini}} = 4.6 \times 10^{13}$ m^{-2}. This ρ_{ini}, which corresponds to 40 dislocation sources for a grain with dimensions $d = h = 2000b$, was chosen in order to minimize the dependence on N_0 and to fulfill the condition of multiple source operation (see Fig. 5). It is comparable to experimentally observed dislocation densities [6,30–32]. The data in Fig. 6 are used to deduce the dependence of work hardening and the dependence of stress at a given plastic strain on the film thickness.

4. Discussion

Understanding the plastic deformation of thin polycrystalline fcc metal films requires knowledge about dislocation motion and multiplication in a confined geometry. The analytical model of Nix [34] and Freund [33] predicts the experimentally observed scaling behavior of the flow stress with the inverse film thickness, but gives flow stresses much smaller (by a factor of 4) than measured experimentally for polycrystalline films [1–5,8]. Additional hardening from the interaction of interface dislocations on intersecting slip planes is not sufficient to explain the experimental flow stresses [25,35–37]. Sufficiently high stresses would be required to push a dislocation into an array of interface dislocations on parallel slip planes if the distance between the interface dislocations is small. However, for this configuration the flow stress is only controlled by the distance of the interface dislocations and not by the film thickness, which is in contradiction to experiments [25].

Recently, we proposed that active dislocation sources are rare in thin films and that the activation of dislocation sources is the decisive factor determining the flow stress [8]. We showed that the experimentally determined flow stress of thin films and its scaling with film thickness can be reproduced if the flow stress is identified with the source activation stress. Under the same assumptions, three-dimensional dislocation simulations have now been used to calculate stress–strain curves, which can be compared with experiments.

The simulations mimic a tensile test at room temperature and the results are intended to be compared with the respective experimental data. The micro-tensile experiments were done with copper films deposited on a compliant polyimide substrate [10]. Therefore, the free-standing film configuration was chosen for most of the simulations presented here. The flow stress of capped polycrystalline films is not as different from the flow stress of free-standing polycrystalline films as one would expect from the Nix–Freund model if the grain size is of the same order as the film thickness: if the dislocations can leave the film at the free surface, the activation of the dislocation sources is still impeded by the grain boundaries [7]. Furthermore, even for wafer curvature experiments, where the films are usually deposited on silicon substrates, the condition of impenetrable boundaries seems too severe: some observations show that interface dislocations are not very stable and

disappear after a short time of radiation with the electron beam [27,38–40] or do not form at all [32,41].

4.1. Source-controlled deformation: fewer sources increase work hardening

The operation of a single dislocation source is controlled by the bow out of the pinned segment or the passage of the dislocation between a boundary and a pinning point of the source. The latter is required in order to transform the source back to its initial position to allow further activation [8]. If many sources of different slip systems are present in a grain, dislocations from different sources can interact and the question arises whether the activation of the sources is still the limiting step.

Increasing the number of sources decreases the work hardening as can be seen from the different slopes of the stress–strain curves in Fig. 4. The dependence can be explained by the following argument: If the dislocation sources operate independently of each other, the flow stress should be equal to the activation stress of an average source. The latter is proportional to the number N_{disl} of dislocation loops which have already been produced by the source and are piling up at the boundaries [29, p. 774] divided by the size of a grain d (or h)

$$\sigma \sim \frac{N_{\mathrm{disl}}}{d}. \tag{2}$$

Since

$$\varepsilon_{\mathrm{pl}} \sim \frac{b}{d} N_0 N_{\mathrm{disl}}, \tag{3}$$

the number of loops is proportional to the plastic strain $\varepsilon_{\mathrm{pl}}$ multiplied by d and divided by the number of active dislocation sources, which in turn is approximately proportional to the total number N_0 of sources in the grain. It follows:

$$\sigma \sim \frac{\varepsilon_{\mathrm{pl}}}{N_0}. \tag{4}$$

The $1/N_0$ dependence of the stress can be seen in Fig. 5 (lines) for $N_0 < 60$. This seems to support the assumption of independent source activation. For these N_0 multiple source activation is required to reach appreciable plastic strains, which, however, no longer holds for larger N_0 where a plateau can be observed in Fig. 5.

The importance of interactions between dislocations from different sources can be further investigated by comparing the results of the many-source simulation with the stress–strain curve deduced in Section 3.1 (independent source calculation). Fig. 7 shows both stress–strain curves. The stress of the independent source calculation was multiplied with a Schmid factor of $m = 0.41$, the plastic strain was divided by m in order to compare with the 3D simulation. By choosing the number of dislocations in the independent source calculation as 4.9, both curves can be made to coincide. This shows again that interactions between dislocations from different sources may not be important for the deformation in this thin film geometry.

Furthermore, it can be seen that randomly placed sources are not very efficient in producing plastic strain: only 4.9 optimally placed sources continuously distributed over all sizes produce the same effect as 40 discrete sources in the 3D calculation. This is also illustrated in Figs. 3(c) and (d), which reveal that only a small fraction of sources (in this case nine) have been active. Reasons for inactivity are vanishing Schmid factors, very small source sizes or locations close to boundaries. We conclude that even for the relatively large typical dislocation densities in thin films ($\rho \approx 10^{14}$ m^{-2} [6,30–32]) plastic deformation may be carried by only a few active sources. This is indeed in agreement with in situ TEM observations (see below).

4.2. Comparison of stress–strain curves

In Fig. 8 the simulation is compared with experimental data gained in a micro-tensile test of a copper film on a polyimide substrate [42]. The stress in the film was measured by X-ray diffraction. Only grains with a $\langle 111 \rangle$ orientation were investigated in the data shown [5,10,43]. The film thickness was $h = 1$ μm and the grain size was of similar magnitude. In the computer experiment a free-standing film with $d = h$ and an initial number of sources $N_0 = 160$ was simulated.

For the initial plastic deformation, there is good agreement between experiment and simulation, not only in the stress–strain behavior but also in the dislocation densities, which match reasonably well the dislocation densities determined from the X-ray peak width [42].

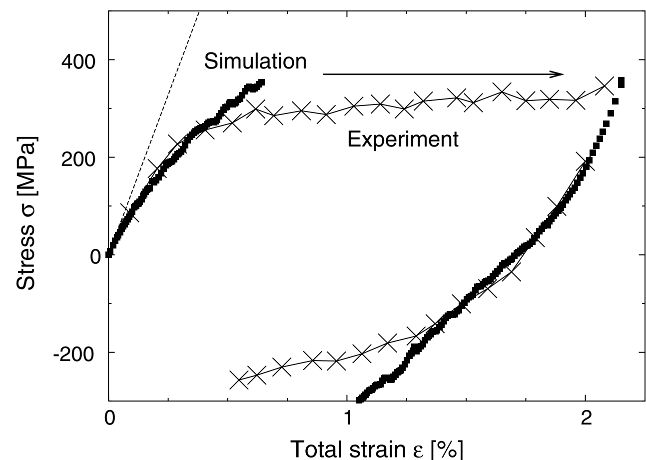

Fig. 8. Stress vs. total strain determined in a micro-tensile test ($h = 1$ μm, $d \approx h$) [42] and in the simulation ($d = h = 1.0$ μm, $N_0 = 160$). The unloading part of the simulated curve has been displaced to larger strains in order to permit a comparison with experiment. The dashed line denotes elastic deformation.

For strains larger than 0.5% the experiment shows a stress plateau, which is not captured by the simulation (compare Fig. 4). This discrepancy must be attributed to relaxation mechanisms which are not implemented in the simulations. Candidates for such relaxation mechanisms are dislocation cross-slip, climb, or transmission of slip through the grain boundaries (Hall–Petch model).

To compare the unloading parts of the stress–strain curves, this part of the simulated curve has been displaced arbitrarily to the right. The experimental and the simulated stress–strain curves then agree well: both show an initial elastic region at the beginning of unloading, and the onset of plasticity already in the tensile region. This Bauschinger type behavior, which is often observed in thin films [11–13], is naturally explained by the source model: when the stress is reduced, the dislocations in the pile-ups move backwards due to their mutual repulsion and annihilate. However, this backwards motion and annihilation does not start immediately at the beginning of the unloading, since the stress to activate the sources is higher than the stress required to push the dislocations against the boundaries.

4.3. Work hardening

Fig. 9 shows the dependence of the hardening rate $H_{pl} = \Delta\sigma/\Delta\varepsilon_{pl}$ on the film thickness deduced from different experiments and from the simulation. The hardening rate was determined in micro-tensile tests from the stress difference at 0.1% and 0.2% plastic strain, where the hardening rate is approximately linear. In wafer curvature experiments the hardening rate was deduced

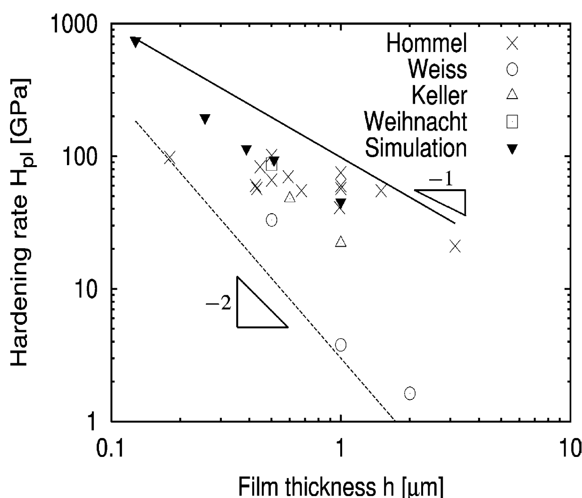

Fig. 9. Simulated and experimental hardening rates vs. film thickness for un-capped copper films. The experimental data are deduced from micro-tensile tests (Hommel [10,57]) and wafer curvature experiments (Weiss [44,58], Keller et al. [4], Weihnacht and Brückner [9]), where the latter are rescaled to a uniaxial stress state. The lines indicate different scaling dependencies.

from the slope of the cooling curve between $T = 250$ and 100 °C. For these temperatures diffusion processes are believed not to contribute to the plastic strain rate [5,44] and the plastic deformation is carried exclusively by gliding dislocations. For biaxial loading (wafer curvature experiments) the resolved shear stress which acts on the moving dislocations is smaller than for uniaxial loading at the same applied stress. Additionally, the component of the plastic strain in loading direction caused by moving dislocations is smaller under biaxial stress. Both effects cause higher hardening rates in wafer curvature experiments which in each case corresponds to the ratio of the Schmid factors m_{bi}/m_{uni}. To display both hardening rates in the same diagram Fig. 9, the wafer curvature data were scaled with the square of the ratio of the Schmid factors $(m_{bi}/m_{uni})^2 \approx (0.27/0.4)^2$. Thermal activation and temperature dependence of the elastic constants was not accounted for.

An increase of the experimentally determined hardening rates with decreasing film thickness is evident in Fig. 9. The scaling dependence lies between $1/h$ and $1/h^2$ for film thicknesses larger than 0.5 µm and possibly saturates at lower thicknesses. The $1/h$ and $1/h^2$ dependencies can be motivated following the argument given in Section 4.1. If as a first-order approximation the number of active dislocation sources is taken to be independent of stress and if the flow stress is identified with the source activation stress, the flow stress can be approximated with Eq. (4). The change of the hardening with film thickness then only depends on the change of the number of dislocation sources per grain N_0 with film thickness. Assuming that dislocation sources emerge from an initial dislocation density in the grain interior (dislocation length per volume) which is independent of grain size and film thickness, a $N_0 \sim h^2$ dependence follows. However, if the number of dislocation sources depends on a constant density of line defects in the grain boundaries (length of grain boundary ledges per area), a $N_0 \sim h$ scaling is obtained. Hardening rates deduced from the independent source calculation (Section 3.1) confirm these scaling laws. A constant density of sources per area results in a $1/h^2$ dependence of the hardening rate.

The simulated data points were deduced from stress–strain curves for the free-standing film geometry (Fig. 6). A constant initial dislocation density $\rho_{ini} = 0.46 \times 10^{14}$ m^{-2} was used and the hardening rates were calculated from the difference in stress between $\varepsilon_{pl} = 0.2\%$ and 0.4% plastic strain. For small film thicknesses, a $1/h^2$ dependence of the hardening rate is observed as expected from the argument given above. For larger film thicknesses a relatively higher hardening is noticed. In contrast to thinner films, where the number of active dislocation sources is constant when going from $\varepsilon_{pl} = 0.2\%$ to $\varepsilon_{pl} = 0.4\%$, N_0 increases within this interval for the $d = h = 1$ µm grain: the larger the grain

dimensions, the less dislocation loops per source are necessary to achieve a given plastic strain as can be seen from Eq. (3) with $N_0 \sim h^2$. In addition, dislocation short range interaction impede the source activation in this initial stage of the deformation. Therefore, at small plastic strains, not every dislocation source has emitted at least one loop and a higher hardening rate than predicted by Eq. (4) is caused.

To conclude, the dependence of the hardening rate on the film thickness depends strongly on the change of the number of dislocation sources in the grain. The number of dislocation sources is not known, and a constant dislocation density was chosen in the simulation as a first guess. Using this assumption, the simulation matches the experimental data reasonably well and a decrease of the hardening rate with increasing grain dimensions is found; however, the scatter in the experimental data is very large and the scaling dependence on the film thickness cannot be identified without ambiguity from these experiments.

4.4. Dependence of flow stress on film thickness

Fig. 10 displays the thickness dependence of the flow stress for experiment and simulation. The wafer curvature data are the stresses at the low temperature end (~40 °C) of the wafer curvature cycles. To compare these data with the micro-tensile test data and the simulations, the plastic strain of the wafer curvature experiments has to be estimated: assuming that dislocation slip is the dominant deformation mechanisms below temperatures of 250 °C (where stress–temperature cycles show a pronounced increase in the hardening rate), a total strain of $\Delta\alpha\,\Delta T = 0.3\%$ is expected to result from cooling to 40 °C due to the difference in thermal expansion coefficients of the copper film and silicon substrate of $\Delta\alpha = 1.41 \times 10^5\ \mathrm{K}^{-1}$. Subtracting the elastic strain due to a stress increase of approximately 300 MPa during cooling, a plastic strain of 0.2% follows. This is equivalent to a plastic strain of roughly 0.3% under uniaxial tension if the difference in Schmid factors is taken into account. The wafer curvature stresses, which are scaled with the ratio of the Schmid factors ($m_{\mathrm{bi}}/m_{\mathrm{uni}} = 0.675$) to account for the different stress states, are comparable to the micro-tensile stresses at 0.2%. At 0.2% plastic strain, a pronounced work hardening is still observed in the stress–strain curves of micro-tensile experiments (Fig. 6) whereas at strains larger than 0.5% they show a plateau region. This apparently is in contrast to wafer curvature experiments, where the stress is reported to decrease linearly upon cooling below room temperature with no indication for a plateau region [9,13]. The reason for the different deformation behavior is not yet understood, probably it is caused by the different interfaces to the substrate: thin films used in micro-tensile tests are deposited on a compliant substrate (polyimide) and the obstacle strength of the interfaces might be weaker than in wafer curvature samples where the films are deposited on rigid substrates (silicon). During the deformation, the dislocations pile-up at the grain boundaries and interfaces. According to the Hall–Petch model, the grain boundaries become permeable if the stress exerted on the boundaries exceeds a certain level. The transmission of slip to the substrate is not possible. Therefore, at further straining only the dislocations at the interface will contribute to the work hardening and a strong influence of the nature of the interface on the hardening rate is expected.

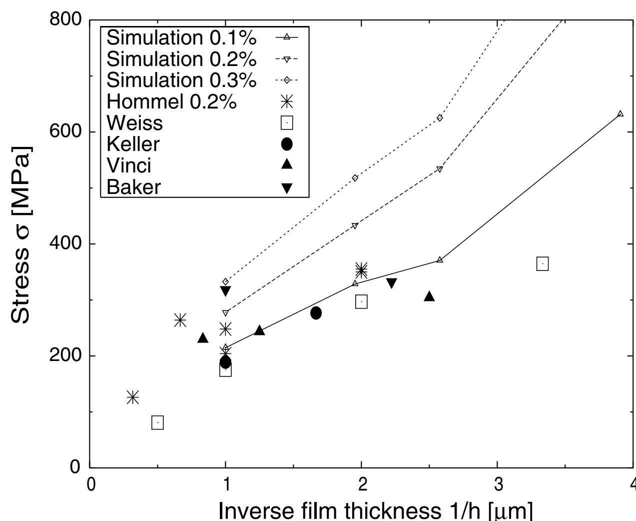

Fig. 10. Flow stress vs. inverse film thickness. The simulation was performed for a free-standing film with an initial dislocation density of $\rho_{\mathrm{ini}} = 0.46 \times 10^{14}\ \mathrm{m}^2$. The experimental data is taken from wafer-curvature experiments (Vinci et al. [3], Keller et al. [4], Weiss [44,58], Baker et al. [28]) and micro-tensile tests (Hommel [10,57]), for uncapped copper films. The wafer curvature stresses are scaled with the ratio of the corresponding Schmid factors to permit a comparison with the micro-tensile tests.

Qualitatively, the simulated stresses are in good agreement with the experimental data and the scaling with the film thickness can be reproduced. The simulation shows a $1/h$ dependence of the flow stress at the same plastic strain if a constant source density is used, except for very small film thicknesses ($d = h = 256$ nm), where the stress increases sharply. Here, the number of dislocation sources is so small, that no source exists in a favorable position (see Section 4.1). At large plastic strains, the stresses predicted by the simulation are higher than the experimental data. This is expected, because no relaxation mechanisms are implemented in the simulation. In contrast to other thin film models (Nix–Freund model [33,34], Thompson model [45]), which predict flow stresses much smaller than observed, the assumption of source controlled deformation, can explain high flow stresses.

4.5. Comparison with TEM observations

The simulations are based on the existence of dislocation sources or multiplication sites in the grain and have suggested that thin film plasticity is largely controlled by source operation. These general findings appear to be consistent with results of in situ TEM studies. For example, dislocation loops were observed to emerge in the grain interior and to move outwards during the deformation of copper films on silicon substrates in cross-section [32,41]. Jerky dislocation motion, which was found in thin copper films [31,41], can be attributed to dislocation obstacles in the grains. This kind of dislocation motion was also seen in the simulation, where dislocations stay in their critical configuration for a long time and move abruptly to the boundaries if the stress is high enough to pass the critical configuration. The sudden movement over long distances is an indication for strong obstacles and was also noticed in in situ TEM studies [46].

In the simulation the first dislocation loops are produced by sources whose slip systems have a high Schmid factor. Because of large back-stresses of the dislocations which pile-up at the boundaries, these sources cease to operate and sources with lower Schmid factors become active. A similar behavior was observed in a TEM study of the active slip systems in a thin Al–Cu film [47]. The simulation also shows that the dislocation density at the grain boundaries is higher than in the grain interior after the film has been deformed (Fig. 3). Similar dislocation distributions have been found in polycrystalline thin copper films [10].

The observation of reversible dislocation structures during cyclic loading [38,48,49] also provides evidence for a limited number of active dislocation sources in polycrystalline thin films. A chaotic, non-reversible dislocation pattern formation would be expected for an unlimited number of sources [50]. Furthermore, a small number of dislocation sources gives rise to inhomogeneous deformation and inhomogeneous stress distribution, which was also found by micro-diffraction [51].

Finally, we note that source controlled deformation seems to apply to polycrystalline thin films with high dislocation densities ($\rho \sim 10^{14}$ m^{-2} [6,30–32]), whereas epitaxially grown copper films are well described by the Nix–Freund model [52]. In the latter case, the dislocation density within the film is much lower. A network of misfit dislocations exists in the interface which accommodates the mismatch in the lattice constants of film and substrate. This network can emit dislocations into the film [52] and dislocation creation and multiplication does not seem to be the critical step in the deformation of epitaxially grown films.

Whereas both limiting cases for the interface, impenetrable obstacles and free surfaces, were considered, the strength of the grain boundaries was not varied in the presented simulations. It is evident that the boundaries do obstruct the dislocation motion, otherwise the high flow stresses of polycrystalline thin films would not be observed, but, obviously some mechanisms have to exists which reduce the stress concentrations of pile-ups at the grain boundaries. Here, only the initial phase of the deformation where strong work hardening takes place, could be simulated. Efforts to include grain boundary strength in analogy to the Hall–Petch model in the simulation and to investigate the plastic deformation of a grain ensemble are currently underway.

5. Summary

The plastic deformation of a polycrystalline thin film of a fcc metal was simulated by considering the dislocation motion in a columnar grain. The dislocations were introduced by randomly placing Frank–Read sources inside the crystal. The grain boundaries were treated as impenetrable obstacles. Stress–strain curves were calculated and compared with experimental data. The following findings were made:

1. If dislocation sources exist in the grain interior, the activation of these sources is the most difficult step in the deformation process. The simulations show an inverse dependence of the flow stress on film thickness, except for very small grains (grain size or thickness below 250 nm) where a strong stress increase is found due to the small number of dislocation sources per grain. Interaction between dislocations from different sources are only of minor importance in thin films but influence work hardening in thicker films.
2. The initial deformation regime of micro-tensile tests can be reproduced well with the simulations. However, the plateau regime in the stress–strain curves of micro-tensile tests at larger strains cannot be captured since no relaxation mechanisms are incorporated in the simulation.
3. The work hardening in thin films can be explained by the back stress of dislocations on their respective sources. The dependence of the hardening rate on film thickness can be reproduced by using an initial dislocation source density independent of grain dimensions.
4. Many features seen in the simulation have also been observed in TEM studies. Nevertheless further in situ studies of dislocations in thin films are required in order to verify source controlled deformation mechanism of thin films, on which these simulations are based.

Acknowledgements

This work was financially supported by the Deutsche Forschungsgemeinschaft (Gu 367/18).

Appendix A. Short-range interaction

Short range interactions between dislocations are calculated on the basis of linear elasticity. A cut-off distance of one Burgers vector for the mutual interaction is introduced. For closer distances the interaction stress is assumed to remain at the value calculated for one Burgers vector distance.

Attractive dislocations with the same Burgers vector recombine. Dislocation junctions can form if two attractive dislocations on different slip planes align along the line of intersection of the slip planes. A replacement of the aligned dislocations with a new reaction–product segment is not required since the far field of the two aligned dislocation segments is identical to the stress field of a dislocation with the combined Burgers vector. In order to save computing time, only the nodes at both ends of the dislocation junction are explicitly kept in the calculation (12).

If it is detected that two repulsive dislocations on different slip planes will collide, a special collision node is placed on the line of intersection of the slip planes (Fig. 11). This collision node ensures that the two dislocations pass each other only if the force in forward direction becomes larger than the mutual repulsion. The creation of jogs in the cutting process of two dislocations is neglected because the force needed to move a jog at room temperature is much smaller than the elastic interaction between dislocations [53, p. 223].

Attractive interactions between dislocations form strong obstacles and an accurate treatment of these obstacles is required in order to simulate work hardening. To check the code, test calculations of the formation and destruction of dislocation junctions under an applied stress have been performed and compared with line tension calculations and other simulations. The (reduced) stress $2\tau L/(\mu b)$ to open a dislocation junction of two dislocations in the configurations of Fig. 12 is displayed in Fig. 13 as a function of the inclination angle φ of the forest dislocation with respect to the line of intersection of the two slip planes. The distance of the pinning points of the mobile dislocation is $2L$, the length of the forest dislocation is L. τ is the resolved shear stress acting on the mobile dislocation, μ the shear modulus and b the magnitude of the Burgers vector. The results are compared with line tension calculations by Schoeck and Frydman [54]. Regarding the severe approximations made in the line tension calculation (neglect of the interaction between remote parts of the dislocations, simplifying description of the shape of the dislocations, use of a different cut-off procedure in calculating the stresses) the consistence is satisfactory.

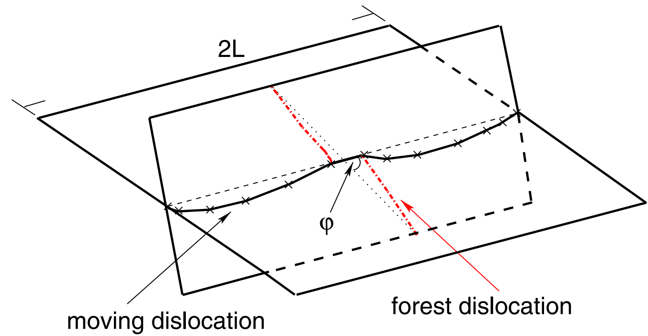

Fig. 12. Two attractive dislocations on different slip planes align along the line of intersection of the planes and form a dislocation lock. The configuration shown is chosen for the test calculations presented in Fig. 13. The slip system of the forest dislocation is $(\bar{1}\,\bar{1}\,1)[\bar{1}\,0\,\bar{1}]$. φ is the angle between the initial line direction of the forest dislocation and the line of intersection of the two slip planes ($[1\,\bar{1}\,0]$ direction). The initial line direction of the mobile dislocation is $[1\,\bar{1}\,0]$, its Burgers vector is parallel to the dislocation line, the slip plane is $(1\,1\,1)$. The dislocations are pinned at their end points.

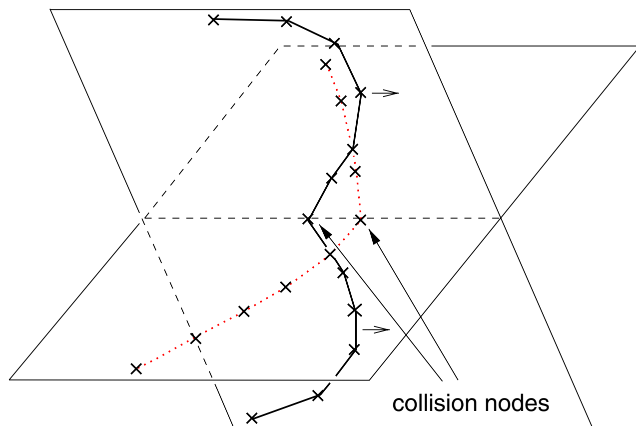

Fig. 11. Illustration of a dislocation cutting process. The moving direction of one dislocation is indicated by arrows.

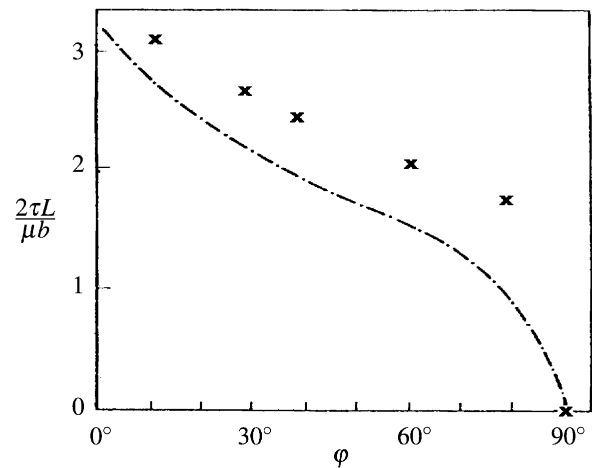

Fig. 13. Comparison of the reduced stress required to unzip the junction $2\tau L/(\mu b)$ with line tension calculations from Schoeck and Frydman [54] (line) for the configuration shown in Fig. 12. τ is the resolved shear stress acting on the mobile dislocation. The forest dislocation does not experience a force due to the applied stress.

Shenoy et al. [55] calculated the stress to unzip a junction for a configuration where the angle of both dislocations with the line of intersection of the slip planes is 60° and the initial lengths of the dislocations equal $2L$. Their dislocation simulation treats partial dislocations which are bound by a stacking fault. They found a critical stress of $\tau_c = 0.64\mu b/L$ if the same resolved shear stress acts on both dislocations. Using our code which considers only perfect dislocations we found a critical stress of $\tau_c = 0.7\mu b/L$. These results are in good agreement, and larger than the predictions based on line tension calculations ($\tau_c \approx 0.5\mu b/L$ [55]). In an atomistic simulation [56] a critical stress of $\tau_c = 0.8\mu b/L$ was found for the case where the resolved shear stress on one dislocation is larger than the resolved shear stress on the other dislocation by a factor of 1.3. This agreement between atomistic and dislocation simulations of the unzipping process of the junction is regarded as very good.

References

[1] Murakami M. Thin Solid Films 1979;59:105.
[2] Venkatraman R, Bravman JC. J Mater Res 1992;7:2040.
[3] Vinci RP, Zielinski EM, Bravman JC. Thin Solid Films 1995;262:142.
[4] Keller R-M, Baker SP, Arzt E. J Mater Res 1998;13:1307.
[5] Kraft O, Hommel M, Arzt E. Mater Sci Eng A 2000;288:209.
[6] Keller RR, Phelps JM, Read DT. Mater Sci Eng A 1996;214:42.
[7] von Blanckenhagen B, Gumbsch P, Arzt E. Mater Res Soc Symp Proc 2001;673:P2.3.1.
[8] von Blanckenhagen B, Gumbsch P, Arzt E. Phil Mag Lett 2003;83:1.
[9] Weihnacht V, Brückner W. Acta Mater 2001;49:2365.
[10] Hommel M, Kraft O. Acta Mater 2001;49:3935.
[11] Kretschmann A, Kuschke WM, Baker SP, Arzt E. Mater Res Soc Symp Proc 1997;436:59.
[12] Baker SP, Keller R-M, Arzt E. Mater Res Soc Symp Proc 1998;505:606.
[13] Shen Y-L, Suresh S, He MY, Bagchi A, Kienzle O, Rühle M, Evans AG. J Mater Res 1998;13:1928.
[14] Kubin LP, Canova G, Condat M, Devincre B, Pontikis V, Bréchet Y. Solid State Phenom 1992;23 & 24:455.
[15] Brown LM. Phil Mag A 1967;15:363.
[16] Schwarz KW. J Appl Phys 1999;85:108.
[17] Devincre B, Condat M. Acta Metall Mater 1992;40:2629.
[18] von Blanckenhagen B, Gumbsch P, Arzt E. Modelling Simul Mater Sci Eng 2001;9:157.
[19] Embury JD, Hirth JP. Acta Metall Mater 1994;42:2051.
[20] Nix WD. Scripta Metall 1998;39:545.
[21] Lothe J. In: Simmons JA, de Wit R, Bullough R, editors. Fundamental aspects of dislocation theory, vol. 317. National Bureau of Standards Spec. Publishing; 1970. p. 11–22.
[22] Liu XH, Ross FM, Schwarz KW. Mater Res Soc Symp Proc 2001;673:4.2.1.
[23] Fivel MC, Gosling TJ, Canova GR. Modelling Simul Mater Sci Eng 1996;4:581.
[24] Hartmaier A, Fivel MC, Canova GR, Gumbsch P. Modelling Simul Mater Sci Eng 1999;7:781.
[25] von Blanckenhagen B, Ph.D. Thesis, Versetzungen in dünnen Metallschichten, Universität Stuttgart, 2002. Available from: http://elib.uni-stuttgart.de/opus/volltexte/2002/1127/.
[26] Foreman AJE. Phil Mag A 1967;15:1011.
[27] Venkatraman R, Chen S, Bravman JC. J Vac Sci Technol A 1991;9:2538.
[28] Baker SP, Kretschmann A, Arzt E. Acta Mater 2001;49:2145.
[29] Hirth JP, Lothe J. Theory of dislocations. Malabar: Krieger Publishing Company; 1982.
[30] Keller-Flaig R-M, Legros M, Sigle W, Gouldstone A, Hemker KJ, Suresh S, Arzt E. J Mater Res 1999;14:4673.
[31] Kobrinsky MJ, Thompson CV. Acta Mater 2000;48:625.
[32] Dehm G, Weiss D, Arzt E. Mater Sci Eng A 2001;309:310–468.
[33] Freund LB. J Appl Mech 1987;54:553.
[34] Nix WD. Metall Trans A 1989;20A:2217.
[35] Schwarz KW, Tersoff J. Appl Phys Lett 1996;69:1220.
[36] Gomez-Garcia D, Devincre B, Kubin L. J Comput Aided Mater Design 1999;6:157.
[37] Pant P, Schwarz KW, Baker SP. Mater Res Soc Symp Proc 2001;673:221.
[38] Kuan TS, Murakami M. Metall Trans A 1982;13A:383.
[39] Müllner P, Arzt E. Mater Res Soc Symp Proc 1998;505:149.
[40] Arzt E, Dehm G, Gumbsch P, Kraft O, Weiss D. Prog Mater Sci 2001;46:283.
[41] Dehm G, Arzt E. Appl Phys Lett 2000;77:1126.
[42] Brederek A, Kraft O. Unpublished, 2001.
[43] Hommel M, Kraft O, Arzt E. J Mater Res 1999;14:2373.
[44] Weiss D, Gao H, Arzt E. Acta Mater 2001;49:2395.
[45] Thompson CV. J Mater Res 1993;8:237.
[46] Dehm G. Unpublished, 2002.
[47] Jawarani D, Kawasaki H, Yeo IS, Rabenberg L, Start JP, Ho PS. J Appl Phys 1997;82:171.
[48] Allen CW, Schroeder H, Hiller JM. Mater Res Soc Symp Proc 2000;594:123.
[49] Balk TJ, Dehm G, Arzt E. Mater Res Soc Symp Proc 2001;673:2.1.13.
[50] Deshpande VS, Needleman A, Van der Giessen E. Scripta Metall 2001;45:1047.
[51] Tamura N, Celestre RS, MacDowell AA, Padmore HA, Spolenak R, Valek BC, Chang NM, Manceau A, Patel JR. Rev Sci Instr 2002;73:1369.
[52] Dehm G, Inkson BJ, Balk TJ, Wagner T, Arzt E. Mater Res Soc Symp Proc 2001;673:211.
[53] Friedel J. Dislocations. Oxford: Pergamon Press; 1964.
[54] Schoeck G, Frydman R. Phys Status Solidi B 1972;53:661.
[55] Shenoy VB, Kutka RV, Phillips R. Phys Rev Lett 2000;84:1491.
[56] Rodney D, Phillips R. Phys Rev Lett 1999;82:1704.
[57] Hommel M, Ph.D. Thesis, Röntgenographische Untersuchung des monotonen und zyklischen Verformungsverhaltens dünner Metallschichten auf Substraten, Universität Stuttgart, 1999.
[58] Weiss D, Ph.D. Thesis, Deformation mechanisms in pure and alloyed copper films, Universität Stuttgart, 2000.